Spatial quadratic solitons guided by narrow layers of a nonlinear material

Asia Shapira,* Noa Voloch-Bloch, Boris A. Malomed, and Ady Arie

Department of Physical Electronics, School of Electrical Engineering, Tel Aviv University, Tel Aviv 69978, Israel
**Corresponding author: asiasapi@post.tau.ac.il*

Received February 7, 2011; revised April 16, 2011; accepted April 19, 2011;
posted April 19, 2011 (Doc. ID 142374); published May 19, 2011

We report analytical solutions for spatial solitons supported by layers of a quadratically nonlinear ($\chi^{(2)}$) material embedded into a linear planar waveguide. A full set of symmetric, asymmetric, and antisymmetric modes pinned to a symmetric pair of the nonlinear layers is obtained. The solutions describe a bifurcation of the subcritical type, which accounts for the transition from the symmetric to asymmetric modes. The antisymmetric states (which do not undergo the bifurcation) are completely stable (the stability of the solitons pinned to the embedded layers is tested by means of numerical simulations). Exact solutions are also found for nonlinear layers embedded into a nonlinear waveguide, including the case when the uniform and localized $\chi^{(2)}$ nonlinearities have opposite signs (competing nonlinearities). For the layers embedded into the nonlinear medium, stability properties are explained by comparison to the respective cascading limit.

OCIS codes: 190.5530, 190.4350, 190.4410.

1. INTRODUCTION

The use of composite materials and engineered optical media opens ways to new modes of guided wave propagation, including self-trapped nonlinear ones, in the form of spatial solitons. Recent reviews summarize results obtained along these directions for photonic crystals [1] and quasi-crystals [2], quasi-discrete media [3], and nonlinear lattices, which feature periodic modulation of the local nonlinearity [4].

In ordinary settings, optical solitons are supported by uniform nonlinearities (cubic, quadratic, or saturable), which may be combined with a periodic grating, that plays the role of a linear potential of the lattice type [5], and is necessary for stabilizing solitons against collapse in the multidimensional geometry [6]. On the other hand, spatially modulated nonlinearities may themselves induce an effective potential [4]. In particular, an interesting issue is a possibility to support solitons by localized nonlinearities embedded into linear host media. To introduce the topic, we will resort here to a couple of simple models that admit analytical solutions, and thus provide for a direct insight into specific properties of solitons supported by the localized nonlinearity.

The simplest model of this type was introduced in [7], in the form of the nonlinear Schrödinger (NLS) equation for the wave amplitude $u(x,z)$, with the cubic nonlinearity localized at a single point:

$$iu_z + (1/2)\psi_{xx} + \delta(x)|u|^2u = 0. \tag{1}$$

In terms of the optical transmission, z is the propagation distance and x is the transverse coordinate. Obviously, Eq. (1) amounts to a linear equation at $x<0$ and $x>0$, supplemented by the jump condition for the derivative at $x=0$, which is produced by the integration of the equation around $x=0$:

$$u_x(x=+0)-u_x(x=-0)=-2|u(x=0)|^2u(x=0). \tag{2}$$

A family of exact solutions to Eq. (1), in the form of peakons, is obvious:

$$u(x,z)=(2k)^{1/4}\exp\left(ikz-\sqrt{2k}|x|\right), \tag{3}$$

with arbitrary propagation constant $k>0$. This family features degeneracy, as the power (norm) of the solutions does not depend on k, $P\equiv\int_{-\infty}^{+\infty}|u(x)|^2dx\equiv 1$. In particular, the formal application of the Vakhitov–Kolokolov (VK) criterion, $dP/d\mu<0$, which is a necessary stability condition for solitons in self-focusing nonlinear media [8], predicts neutral stability of Eq. (3). In fact, all these degenerate solitons are unstable, collapsing into a singularity or decaying, as illustrated by another analytical solution to Eq. (1), which explicitly describes the onset of the collapse at $z\to -0$ [9]:

$$\psi(x,z)=\sqrt{-x_0/z}\exp[i(|x|-ix_0)^2/(2z)]. \tag{4}$$

Here $x_0>0$ is an arbitrary real constant, and z is negative. The same Eq. (4) with $x_0<0$ describes decaying solitons at $z>0$ [9]. The power of this solution is also $P=1$, irrespective of the value of x_0.

The solitons may be stabilized if a linear periodic potential is added to Eq. (1) [9]. The stability is also achieved if the single δ function in Eq. (1) is replaced by a symmetric pair, which corresponds to the equation introduced in [10] (see also a related discrete model recently introduced in [11]):

$$iu_z + (1/2)\psi_{xx} + [\delta(x-L/2)+\delta(x+L/2)]|\psi|^2\psi = 0. \tag{5}$$

Exact analytical solutions to Eq. (5) were found in [10] for symmetric, antisymmetric, and asymmetric localized modes. The respective spontaneous-symmetry-breaking (SSB) bifurcation, which generates asymmetric solutions from the symmetric ones, takes place, with the increase of the power, at its critical value $P_{\rm cr}=(8/9)[1+(1/3)\ln 2]\approx 0.95$. In this model,

based on the ideal δ functions, the bifurcation is degenerate, featuring an ultimately subcritical character: branches of the asymmetric solutions go backward as functions of P, up to the state, attained at $P=1$, in which the entire power is concentrated in an infinitely narrow soliton pinned to one of the two δ functions. Accordingly, these branches are fully unstable. The symmetric modes are stable at $P<P_{\rm cr}$ and unstable at $P>P_{\rm cr}$, while antisymmetric modes are completely unstable, although they do not undergo any bifurcation.

The degenerate character of the model with the two ideal δ functions is the price paid for its analytical solvability. The degeneracy is lifted if the δ functions in Eq. (5) are approximated by regular expressions:

$$\delta(x\mp L/2)\to\delta(x\mp L/2)\equiv\frac{1}{\sqrt{\pi}a}\exp\left(-\frac{(x\mp L/2)^2}{a^2}\right), \quad (6)$$

with small regularizing parameter a. The numerical analysis of the regularized model demonstrates that the branches of asymmetric states turn forward at some P, which causes the stabilization of the asymmetric solutions past the turning points. At $a>a_0\approx 0.2$, the SSB bifurcation becomes supercritical, i.e., the branches of the asymmetric solutions go forward immediately after they emerge, being completely stable [10].

Rather than being represented by a single spot or a symmetric pair, as outlined above, the localized nonlinearity may be extended to a periodic lattice of δ functions embedded into the linear medium. The description of stationary modes in such a model can be exactly reduced to stationary solutions of the discrete NLS equation [12,13], which has been studied in detail [14]. However, the periodic nonlinearity does not admit asymmetric modes.

A fundamental role in optics belongs to second-harmonic (SH) generating systems based on the quadratic ($\chi^{(2)}$) nonlinearity [15,16]. In this connection, it is relevant to consider media with one or several narrow $\chi^{(2)}$ layers embedded into a linear planar waveguide. For the single layer approximated by the respective δ function, exact solutions in the form of peakons, similar to those given by Eq. (3), were found in [17]. Unlike the solutions in Eq. (3), they are not degenerate (the total power depends on the propagation constant), a bigger part of the solution family being stable.

A new problem, which is considered in the present work, is to find double peakons pinned to a symmetric pair of $\chi^{(2)}$ delta functions; cf. Eq. (5) for the $\chi^{(3)}$ nonlinearity. In this model, we report analytical solutions of all the types, namely, symmetric, antisymmetric [as concerns the fundamental-frequency (FF) component], and asymmetric ones. The corresponding SSB bifurcation is subcritical, but nongenerate (i.e., asymmetric branches eventually turn forward as stable ones). Antisymmetric modes do not undergo bifurcations, and turn out to be stable.

Another new configuration is a nonlinear double layer (alias a dipolar layer), formed by a fused pair of two narrow nonlinear stripes with opposite signs. While it would be very difficult to create such a configuration for the Kerr nonlinearity, in $\chi^{(2)}$ systems it is more feasible, as the sign of the nonlinearity may be changed by reversing the orientation of ferroelectric domains accounting for the $\chi^{(2)}$ interaction. We consider the double layer described by function $\delta'(x)$ in front of the $\chi^{(2)}$ terms. A family of exact solutions for solitons pinned to the double layer is found, but they all turn out to be unstable (throughout the paper, the stability is tested via direct simulations of the perturbed evolution, in the framework of equations with the ideal δ functions replaced by their regularized counterparts).

The most challenging problem is to construct analytical solutions for a soliton pinned to a nonlinear layer embedded into a nonlinear waveguide. In this setting, the signs of the localized and uniform $\chi^{(2)}$ nonlinearities may be identical or opposite. We produce exact solutions of two different types for this case, and test their stability. We also find some particular exact symmetric solutions for a pair of nonlinear layers inserted into the nonlinear waveguide.

The paper is structured as follows. In Section 2, we briefly recapitulate the peakon solution for the single $\chi^{(2)}$ layer embedded into the linear medium. In particular, we apply the adiabatic approximation to the description of peakons pinned to the layer whose strength slowly varies along the propagation distance. The most essential results are reported in Section 3, dealing with the pair of $\chi^{(2)}$ layers embedded into the linear medium, including exact solutions for asymmetric double peakons. Results for the double layer are presented in Section 4, and the nonlinear layer(s) buried into the nonlinear waveguide are considered in Section 5. The paper is concluded by Section 6.

2. $\chi^{(2)}$ MONOLAYER EMBEDDED INTO THE LINEAR MEDIUM

The basic model, with a single narrow channel carrying the $\chi^{(2)}$ nonlinearity, can be written as follows:

$$i\frac{\partial A_1}{\partial Z}+\frac{1}{2k_1}\frac{\partial^2 A_1}{\partial X^2}+\kappa\delta(X/k_1)A_2A_1^*e^{-i\Delta kZ}=0, \quad (7)$$

$$i\frac{\partial A_2}{\partial Z}+\frac{1}{2k_2}\frac{\partial^2 A_2}{\partial X^2}+\kappa\delta(X/k_1)A_1^2e^{i\Delta kZ}=0, \quad (8)$$

where A_1 and A_2 are local amplitudes of the FF and SH components, k_1 and k_2 are the respective wavenumbers, κ is the nonlinearity coefficient, and Δk is the phase mismatch. To reduce the number of control parameters, we transform Eqs. (7) and (8): $A_1(X,Z)\equiv(1/2)u(x,z)$, $A_2(X,Z)\equiv v(x,z)e^{i\Delta kZ}$, and rescale the spatial coordinates and coefficients by means of k_1, $x\equiv X/k_1$, $z\equiv Z/k_1$, $\gamma=\kappa/k_1$, and $Q=2\Delta k/k_1$. The resulting normalized equations are

$$iu_z+(1/2)u_{xx}+\gamma\delta(x)u^*v=0, \quad (9)$$

$$2iv_z+(1/2)v_{xx}-Qv+(\gamma/2)\delta(x)u^2=0. \quad (10)$$

The integration of the equations in an infinitesimal vicinity of $x=0$ yields the relations for the jumps of gradients of the FF and SH fields at $x=0$ [cf. Eq. (2)]:

$$u_x(x=+0)-u_x(x=-0)=-2\gamma u^*(x=0)v(x=0), \quad (11)$$

$$v_x(x=+0)-v_x(x=-0)=-\gamma u^2(x=0), \quad (12)$$

while the fields themselves must be continuous across $x=0$.

A family of exact stationary solutions to Eqs. (9) and (10) in the form of peakons, similar to Eq. (3), is [17]

$$u_{\rm peak}(z,x) = \pm 2[k(4k+Q)]^{1/4}\gamma^{-1}e^{ikz}\exp\left(-\sqrt{2k}|x|\right),$$
$$v_{\rm peak}(z,x) = \sqrt{2k}\gamma^{-1}e^{2ikz}\exp\left(-\sqrt{2(4k+Q)}|x|\right). \quad (13)$$

Equations (9) and (10) conserve the total power, also known as the Manley–Rowe invariant:

$$P = \int_{-\infty}^{+\infty}[|u(x)|^2dx + 4|v(x)|^2]dx. \quad (14)$$

For peakon Eq. (13), its value is

$$P_{\rm peakon} = 2\sqrt{2}(6k+Q)\left[\gamma^2\sqrt{4k+Q}\right]^{-1}. \quad (15)$$

For $Q<0$, this dependence $P(k)$ has a positive slope, $dP/dk>0$, at $k>-Q/3$, and a negative slope at $0<k<-Q/3$. According to the VK criterion, the peakons should be stable for $k>-Q/3$, and unstable for $0<k<-Q/3$. For $Q>0$, condition $dP/dk>0$ holds for all $k>0$, hence the entire peakon family is expected to be stable for $Q>0$ [17]. It can be verified by direct simulations that the stability of the peakons precisely complies with the predictions of the VK criterion. Note also that Eq. (15) gives rise to a power threshold: the solitons exist if their total power exceeds a minimum value, which vanishes only at $Q=0$:

$$P_{\rm min} = \begin{cases} P(k=0) \equiv 2\sqrt{2Q}/\gamma^2 & \text{for } Q>0, \\ P(k=-Q/3) \equiv 2\sqrt{-6Q}/\gamma^2 & \text{for } Q<0. \end{cases} \quad (16)$$

In the case when the nonlinearity strength slowly varies along the $\chi^{(2)}$ layer, i.e., $\gamma=\gamma(z)$ in Eqs. (9) and (10), the adiabatic approximation may be applied, assuming that the solution given by Eq. (13) remains locally valid at each value of z, with slowly varying $k(z)$, which is determined by the conservation of the total power, $P=$ const. Then, one immediately finds from Eq. (15)

$$k(z) = \frac{1}{4}\left\{\left[\sqrt{\frac{P^2\gamma^4(z)}{72}+\frac{Q}{3}}+\frac{P\gamma^2(z)}{6\sqrt{2}}\right]^2 - Q\right\}. \quad (17)$$

There are limitations on the use of the adiabatic approximation: as seen from Eq. (17), for $Q<0$ this equation makes sense if the expression under the radical is positive, i.e., $\gamma^4(z)>24|Q|/P^2$. For $Q>0$, the radical is always real; however, in that case there is another constraint, $k>0$ [Eq. (13) does not make sense for $k<0$]. As follows from Eq. (17), this constraint amounts to $\gamma^4(z)>8Q/P^2$. Thus, the adiabatic approximation does not allow the peakon to pass points where $\gamma(z)$ vanishes.

3. SYMMETRIC PAIR OF NONLINEAR LAYERS IN THE LINEAR HOST MEDIUM

A. Formulation

The modification of Eqs. (9) and (10) for two parallel layers is obvious; cf. Eq. (5):

$$iu_z + \frac{1}{2}u_{xx} + \gamma\left[\delta\left(x-\frac{L}{2}\right)+\delta\left(x+\frac{L}{2}\right)\right]u^*v = 0, \quad (18)$$

$$2iv_z + \frac{1}{2}v_{xx} - Qv + \frac{\gamma}{2}\left[\delta\left(x-\frac{L}{2}\right)+\delta\left(x+\frac{L}{2}\right)\right]u^2 = 0. \quad (19)$$

Being a novel model for the $\chi^{(2)}$ nonlinearity, it is related to its counterpart in Eq. (5), with the cubic nonlinearity, through the cascading limit, which corresponds to large positive values of mismatch Q [15,16]. In this limit, one can eliminate the SH field, using Eq. (19), $v\approx(\gamma/2Q)[\tilde{\delta}(x-L/2)+\tilde{\delta}(x+L/2)]u^2$, where it is necessary to assume that the ideal δ function is replaced by its regularization $\tilde{\delta}(x)$; see Eq. (6). Then, the substitution of this approximation into Eq. (18) leads to equation

$$iu_z + \frac{1}{2}u_{xx} + \frac{\gamma^2}{2Q}\left[\tilde{\delta}^2\left(x-\frac{L}{2}\right)+\tilde{\delta}^2\left(x+\frac{L}{2}\right)\right]|u|^2u = 0. \quad (20)$$

With the ideal δ function, Eq. (20) does not make sense, as $\delta^2(x)$ does not exist. Nevertheless, if $\tilde{\delta}(x\mp L/2)$ are taken as smooth approximations, Eq. (20) is meaningful, being tantamount to the accordingly regularized version of Eq. (5).

B. General Analysis

Stationary localized solutions to Eqs. (18) and (19) are sought for as

$$u(x,z) = e^{-ikz}\begin{cases} A_-e^{\sqrt{2k}(x+L/2)}, & \text{at } x<-L/2, \\ A_1\cosh\left(\sqrt{2k}x\right)+A_2\sinh\left(\sqrt{2k}x\right), & \text{at } -L/2<x<+L/2, \\ A_+e^{-\sqrt{2k}(x-L/2)}, & \text{at } x>L/2, \end{cases} \quad (21)$$

$$v(x,z) = e^{-2ikz}\begin{cases} B_-e^{\sqrt{2(4k+Q)}(x+L/2)}, & \text{at } x<-L/2, \\ B_1\cosh\left(\sqrt{2(4k+Q)}x\right)+B_2\sinh\left(\sqrt{2(4k+Q)}x\right), & \text{at } -L/2<x<+L/2, \\ B_+e^{-\sqrt{2(4k+Q)}(x-L/2)}, & \text{at } x>L/2. \end{cases} \quad (22)$$

Conditions of the continuity of u and v at $x = \pm L/2$ make it possible to express the inner amplitudes, $A_{1,2}$ and $B_{1,2}$, in terms of the outer ones, $A_{\pm}$ and $B_{\pm}$:

$$A_1 = \frac{A_+ + A_-}{2\cosh\left(\sqrt{k/2}L\right)},$$
$$A_2 = \frac{A_+ - A_-}{2\sinh\left(\sqrt{k/2}L\right)},$$
$$B_1 = \frac{B_+ + B_-}{2\cosh\left(\sqrt{(4k+Q)/2}L\right)},$$
$$B_2 = \frac{B_+ - B_-}{2\sinh\left(\sqrt{(4k+Q)/2}L\right)}. \tag{23}$$

Further, we introduce notations

$$s_1 = \left[\sinh\left(\sqrt{2k}L\right)\right]^{-1}, \qquad s_2 = \left[\sinh\left(\sqrt{2(4k+Q)}L\right)\right]^{-1},$$
$$c_1 = 1 + \coth\left(\sqrt{2k}L\right), \qquad c_2 = 1 + \coth\left(\sqrt{2(4k+Q)}L\right),$$
$$\gamma_1 = \gamma/\sqrt{2k}, \qquad \gamma_2 = \gamma/\sqrt{2(4k+Q)}. \tag{24}$$

Then, the conditions in Eqs. (11) and (12) for the jump of the wave functions at points $x = \pm L/2$ give rise to the following equations:

$$c_1A_- - s_1A_+ = 2\gamma_1A_-B_-, \qquad c_1A_+ - s_1A_- = 2\gamma_1A_+B_+, \tag{25}$$

$$c_2B_- - s_2B_+ = \gamma_2A_-^2, \qquad c_2B_+ - s_2B_- = \gamma_2A_+^2. \tag{26}$$

Using Eq. (26), one can eliminate $B_{\pm}$ in favor of $A_{\pm}$:

$$B_+ = \frac{\gamma_2(c_2A_+^2 + s_2A_-^2)}{c_2^2 - s_2^2}, \qquad B_- = \frac{\gamma_2(c_2A_-^2 + s_2A_+^2)}{c_2^2 - s_2^2}. \tag{27}$$

C. Symmetric, Asymmetric, and Antisymmetric Modes

Substituting Eq. (27) into Eq. (25) and assuming $A_+^2 - A_-^2 \neq 0$ (i.e., that the solution is asymmetric) leads to the following expressions for the amplitudes of the asymmetric modes:

$$A_+A_- = \frac{(c_2 + s_2)s_1}{2\gamma_1\gamma_2}, \qquad A_+^2 + A_-^2 = \frac{c_1}{2c_2}\frac{c_2^2 - s_2^2}{\gamma_1\gamma_2}. \tag{28}$$

The asymmetry of the stationary mode is characterized by

$$\epsilon \equiv \frac{(A_+ - A_-)^2}{(A_+ + A_-)^2} = \frac{c_1c_2 - c_1s_2 - c_2s_1}{c_1c_2 - c_1s_2 + c_2s_1}. \tag{29}$$

On the other hand, Eqs. (25) and (26) immediately give rise to the symmetric solutions:

$$A_+ = A_- \equiv (A_\pm)_{\text{symm}} = \sqrt{\frac{(c_1 - s_1)(c_2 - s_2)}{2\gamma_1\gamma_2}},$$
$$B_+ = B_- \equiv (B_\pm)_{\text{symm}} = (2\gamma_1)^{-1}(c_1 - s_1). \tag{30}$$

Then, Eq. (23) yields, for the symmetric solution, $(A_2)_{\text{symm}} = (B_2)_{\text{symm}} = 0$, and

$$(A_1)_{\text{symm}} = \frac{(A_\pm)_{\text{symm}}}{\cosh\left(\sqrt{k/2}L\right)},$$
$$(B_1)_{\text{symm}} = \frac{(B_\pm)_{\text{symm}}}{\cosh\left(\sqrt{(4k+Q)/2}L\right)}. \tag{31}$$

The asymmetric solutions emerge, with the increase of L, from the symmetric one as a result of the SSB bifurcation, at the point at which the asymmetric solution, as given by Eq. (28), coincides with its symmetric counterpart in Eq. (30). Setting, accordingly, $\epsilon = 0$ in Eq. (29) predicts the location of the bifurcation point: $c_1c_2 = c_1s_2 + c_2s_1$. Only the symmetric solution, given by Eqs. (30) and (31), exists at

$$c_1c_2 < c_1s_2 + c_2s_1, \tag{32}$$

where Eq. (29) formally yields $(A_+ - A_-)^2 < 0$, while both the symmetric and asymmetric solutions exist at

$$c_1c_2 > c_1s_2 + c_2s_1, \tag{33}$$

when Eq. (29) yields $(A_+ - A_-)^2 > 0$.

As follows from the definitions in Eq. (24), the condition in Eq. (32) holds in the limit when the two layers merge into one, $L \to 0$, in which case $c_1 \approx s_1$ and $c_2 \approx s_2$. On the other hand, at $L \to \infty$, the definitions in Eq. (24) imply $c_1 \approx c_2 \approx 2$ and $s_{1,2} \to 0$, i.e., the condition in Eq. (33) holds in the limit of a very large separation between the layers. Therefore, the SSB indeed occurs, with the increase of L, at a particular value of the separation.

It is also possible to find solutions that are antisymmetric in the FF component, with $A_+ = -A_-$ and $B_+ = +B_-$, while the SH component remains symmetric. In this case, Eqs. (23), (25), and (26) yield

$$A_+ = -A_- \equiv (A_\pm)_{\text{antisymm}} = \sqrt{\frac{(c_1 + s_1)(c_2 - s_2)}{2\gamma_1\gamma_2}},$$
$$B_+ = B_- \equiv (B_\pm)_{\text{antisymm}} = (2\gamma_1)^{-1}(c_1 + s_1), \tag{34}$$

$$(A_2)_{\text{antisymm}} = \frac{(A_\pm)_{\text{antisymm}}}{\sinh\left(\sqrt{k/2}L\right)},$$
$$(B_1)_{\text{antisymm}} = \frac{(B_\pm)_{\text{antisymm}}}{\cosh\left(\sqrt{(4k+Q)/2}L\right)}, \tag{35}$$

and $(A_1)_{\text{antisymm}} = (B_2)_{\text{antisymm}} = 0$; cf. Eqs. (30) and (31).

D. Numerical Results

The numerical analysis of the dual-layer model aimed to address two issues: the form of the bifurcation diagram (subcritical or supercritical), which is implicitly described by the above analytical expressions, and the stability of the symmetric, asymmetric, and antisymmetric double peakons.

We took values of rescaled constants and variables that correspond to $k = 1$ and the following typical values of physical parameters: at the FF wavelength of 1.0645 μm, the sample was assumed to be stoichiometric lithium tantalate with the e–ee interaction, where two extraordinary waves induce an

extraordinary nonlinear polarization. Undoing the rescalings that lead to the rescaled notation, it is straightforward to see that rescaled mismatch $Q = 1$ corresponds, in physical units, to a very small value, $6\,\mathrm{m}^{-1}$, i.e., our actual results correspond to the nearly matched $\chi^{(2)}$ system.

Further, the refractive indices and the relevant element of the $\chi^{(2)}$ susceptibility tensor were taken according to [18] (at 100 °C, $n_{\mathrm{FF}} = 2.1323$, $n_{\mathrm{SH}} = 2.1999$, and $d_{33} = 12.9\,\mathrm{pm/V}$). In the simulations of the evolution of perturbed solutions, the δ functions were replaced by the approximation in Eq. (6) with a of a few micrometers. Finally, taking into account the experimentally measured value of the Kerr coefficient in this material, $n_2 \approx 14.6 \times 10^{-16}\,\mathrm{cm}^2/\mathrm{W}$ [19], it is easy to check that, for the physical parameters adopted in this work, the $\chi^{(3)}$ nonlinearity is negligible in comparison with the $\chi^{(2)}$ effects.

Typical examples of stable symmetric, asymmetric, and antisymmetric solitons are displayed in Figs. 1–3, respectively. Additional simulations, with strong perturbations added to the input fields (not shown here), demonstrate that, as it might be expected, the symmetric solitons are stable before the SSB point and unstable past it. The simulations also demonstrate that the antisymmetric solitons are always stable. The stability of asymmetric solitons is discussed below.

Making use of Eqs. (23)–(29) to find the asymmetry ϵ, and calculating the total power of the solutions as per Eq. (14), the bifurcation diagrams were drawn in the plane of (P, ϵ), at different values of mismatch Q. Typical examples of the diagrams, displayed in Fig. 4, clearly demonstrate the subcritical character of the SSB bifurcation, similar to what was found in the model in Eq. (5) with the cubic nonlinearity, which corresponds to the cascading limit of the present system. However,

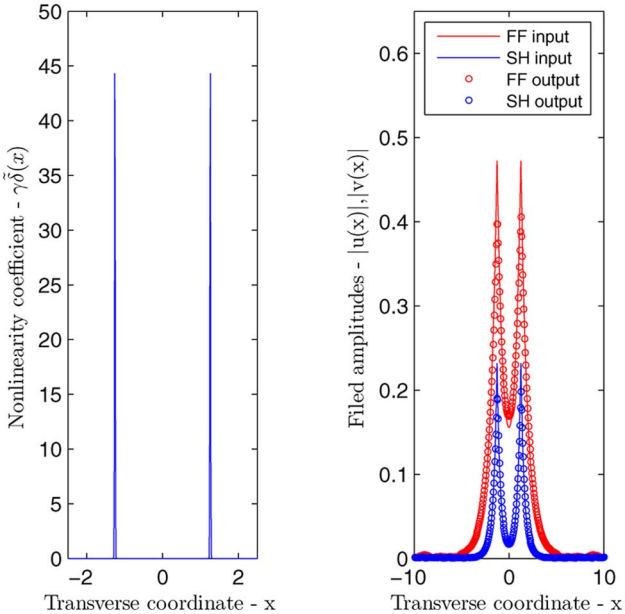

Fig. 1. (Color online) Left, the double-barrier structure corresponding, in physical units, to separation $L = 200\,\mu$m between the two symmetric $\chi^{(2)}$ layers of width $a = 0.92\,\mu$m each. Right, a typical example of stable symmetric solitons. The red (taller) and blue (lower) solid curves depict, respectively, the input for the FF and SH fields, taken as per the analytical solution given by Eqs. (21)–(27) and (30). Chains of dots depict the output produced by simulations of Eqs. (18) and (19), with the δ functions approximated as per Eq. (6), over the propagation distance corresponding to $z = 100\,$cm, in physical units. For this and other examples, the scaled wavenumber of the analytical solutions is taken as $k = 1$. In the present case, the mismatch is $Q = 0$.

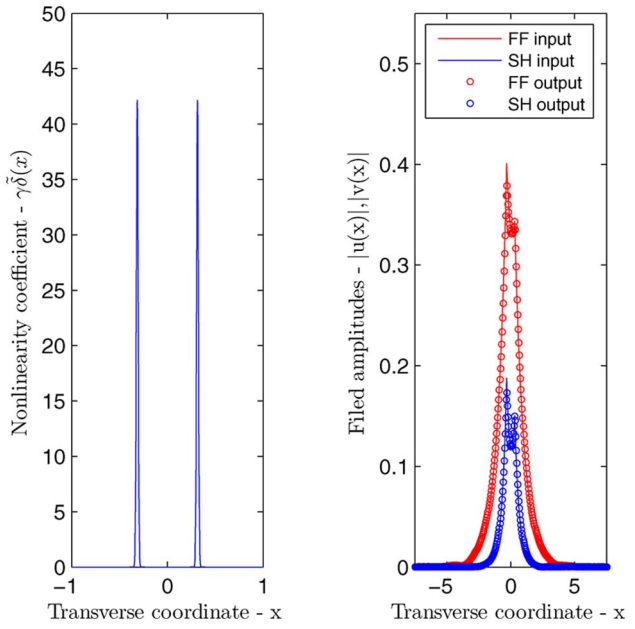

Fig. 2. (Color online) Same as in Fig. 1, but for a stable asymmetric soliton, with $L = 50\,\mu$m, $a = 1.06\,\mu$m, and $z = 10\,$cm.

unlike that model, the present one, even with the ideal δ functions, is not degenerate, i.e., the branches of the asymmetric solutions go forward after reaching the turning point. In accordance with general properties of the symmetry-breaking bifurcations [20], one should expect that branches of the asymmetric solitons corresponding to $d\epsilon/dP > 0$ and $d\epsilon/dP < 0$ should be stable and unstable, respectively. This expectation was confirmed by direct simulations. In particular, all the asymmetric solitons belonging to the positive-slope branch of the $\epsilon(P)$ dependence are stable (Fig. 2 shows an example of such a stable soliton), while a typical example of the instability of the branches with the negative slope is displayed in Fig. 5.

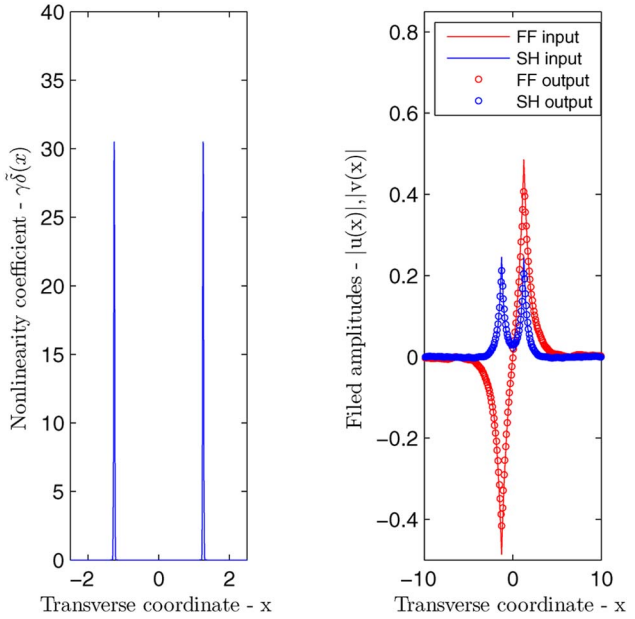

Fig. 3. (Color online) Same as in Figs. 1 and 2, but for a stable antisymmetric soliton, with $L = 200\,\mu$m, $a = 1.4\,\mu$m, and $z = 100\,$cm.

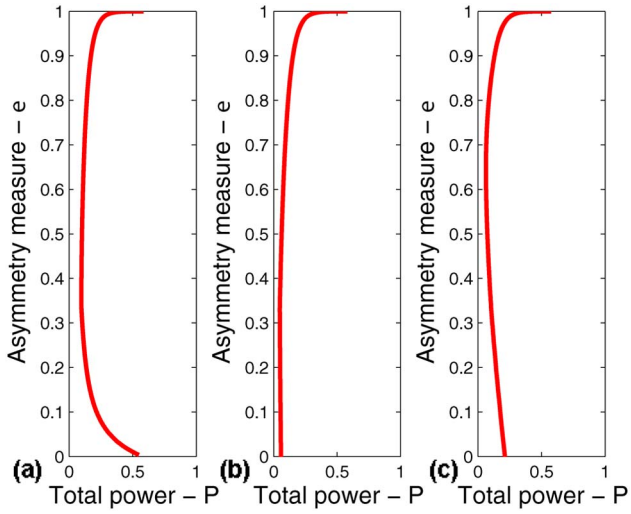

Fig. 4. (Color online) Asymmetry parameter of the solitons versus the total power [defined as per Eq. (29)], for positive, zero, and negative mismatch: (a) $Q = +1$, (b) $Q = 0$, and (c) $Q = -1$.

4. MODEL WITH THE DOUBLE NONLINEAR LAYER

A narrow double layer is formed by two adjacent monolayers with opposite signs of the $\chi^{(2)}$ coefficients. Accordingly, Eqs. (9) and (10) are replaced by

$$iu_z + (1/2)u_{xx} + \gamma\delta'(x)u^*v = 0, \tag{36}$$

$$2iv_z + (1/2)v_{xx} - Qv + (\gamma/2)\delta'(x)u^2 = 0. \tag{37}$$

An exact stationary solution to Eqs. (36) and (37) can be found in the form of antisymmetric discontinuous solitons; cf. the expressions in Eq. (13) for the peakons:

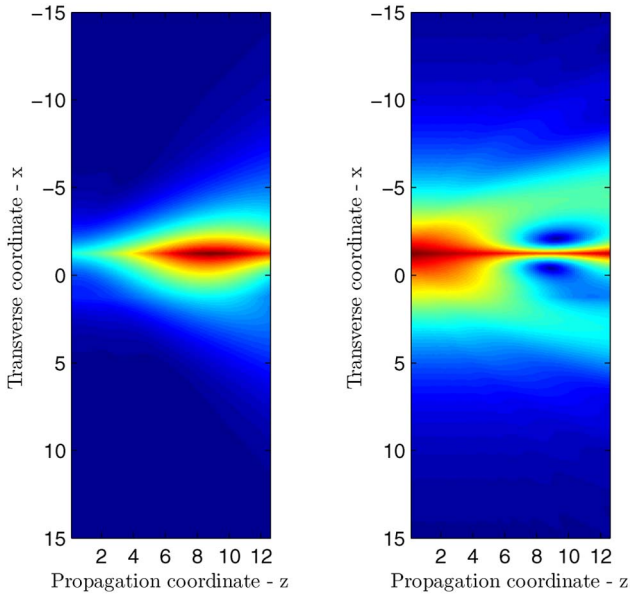

Fig. 5. (Color online) Typical example of the evolution of an unstable asymmetric soliton belonging to the solution branch with $d\epsilon/dP < 0$, is displayed by means of contour plots of local powers of the FF and SH components in the (z,x) plane. The corresponding physical parameters are: $a = 1.4\,\mu$m, $L = 200\,\mu$m, and the total propagation distance is $z = 100$ cm. The rescaled mismatch and wavenumber are $Q = -1$ and $k = 0.26$.

$$u(z,x) = \pm\sqrt{2}\gamma^{-1}e^{ikz}\mathrm{sgn}(x)\exp\left(-\sqrt{2k}|x|\right),$$
$$v(z,x) = -\gamma^{-1}e^{2ikz}\mathrm{sgn}(x)\exp\left(-\sqrt{2(4k+Q)}|x|\right). \tag{38}$$

Note that, unlike the peakons, the amplitudes of these solutions do not depend on k.

According to Eq. (14), the total power of the discontinuous soliton is

$$P_{\mathrm{discont}} = \sqrt{2}\gamma^{-1}[k^{-1/2} + 2(4k+Q)^{-1/2}]. \tag{39}$$

Equation (39) does not give rise to any existence threshold, unlike the peakon solutions [cf. Eq. (16)], because $P_{\mathrm{discont}}(k \to \infty) = 0$. Obviously, Eq. (39) leads to $dP/dk < 0$; hence, the VK criterion predicts that the family of the discontinuous solitons is completely unstable. This prediction was confirmed by simulations of the evolution of these solitons; see Fig. 6, where strong instability dominates the propagation of the soliton even over a relatively short propagation distance, $z = 1$ cm.

5. NONLINEAR LAYERS EMBEDDED INTO A NONLINEAR HOST MEDIUM

A. Single Layer

If the host medium is itself nonlinear, Eqs. (9) and (10) are replaced by

$$iu_z + (1/2)u_{xx} + [\Gamma + \gamma\delta(x)]u^*v = 0, \tag{40}$$

$$2iv_z + (1/2)v_{xx} - Qv + (1/2)[\Gamma + \gamma\delta(x)]u^2 = 0, \tag{41}$$

where Γ and γ account for the bulk and localized $\chi^{(2)}$ nonlinearities, respectively, which may have the same or opposite signs, the latter situation corresponding to the competing bulk and localized nonlinearities. Two particular exact solutions

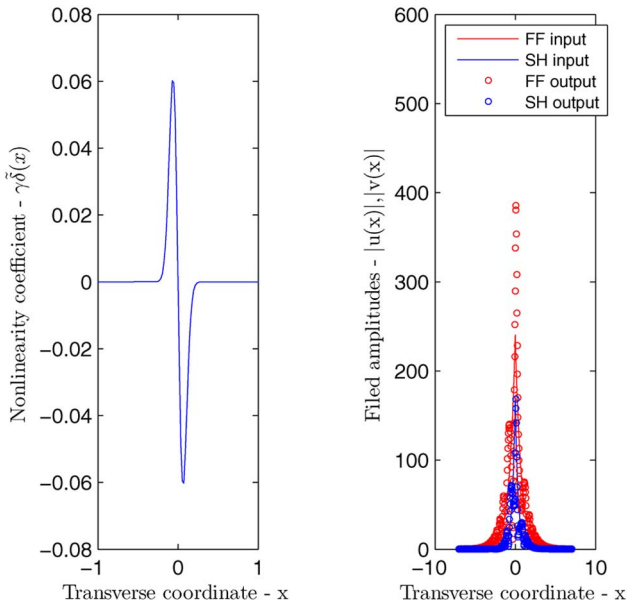

Fig. 6. (Color online) Same as in Figs. 1–3, but for an unstable antisymmetric nearly discontinuous soliton pinned to the double nonlinear layer of width $a = 7.07\,\mu$m, shown in the left panel. In this case, the mismatch is $Q = 0$, the total propagation distance is 1 cm, in physical units, and the scaled value of the initial wavenumber is $k = 1$.

can be found in this model, following the pattern of the well-known Karamzin–Sukhorukov (KS) solutions for $\chi^{(2)}$ solitons in the uniform medium [21].

The first solution is a straightforward extension of the KS soliton, based on the following ansatz:

$$u = e^{ikz} A \mathrm{sech}^2(W(|x| + \xi)), \qquad v = e^{2ikz} B \mathrm{sech}^2(W(|x| + \xi)). \tag{42}$$

Substituting this ansatz into Eqs. (40) and (41) and taking into regard the jump conditions in Eqs. (11) and (12), it is easy to find parameters of the exact solution:

$$k = -Q/3, \qquad W = \sqrt{-Q/6}, \qquad A = \pm\sqrt{2}B, \qquad B = -(Q/2\Gamma), \tag{43}$$

$$\sinh(2W\xi) = \sqrt{-3Q/2}(\gamma/\Gamma). \tag{44}$$

With identical signs of γ and Γ, Eq. (44) yields $\xi > 0$, i.e., a single-hump profile of the pinned soliton in Eq. (42). For opposite signs of γ and Γ, Eq. (44) produces $\xi < 0$, hence the corresponding pinned profile in Eq. (42) features a local minimum at $x = 0$, and two maxima at $x = \pm|\xi|$. The soliton is expected to be stable in the former case, and unstable in the latter one, when it is pinned by the repelling defect in an unstable position. Direct simulations of the evolution of the solitons slightly shifted from the equilibrium positions confirm these expectations. In particular, the instability of the double-humped soliton is illustrated by Fig. 7.

Another type of the pinned soliton can be found in the following form:

$$u = e^{ikz} A' [\sinh(W(|x| + \xi'))]^{-2}, \qquad v = e^{2ikz} B' [\sinh(W(|x| + \xi'))]^{-2}. \tag{45}$$

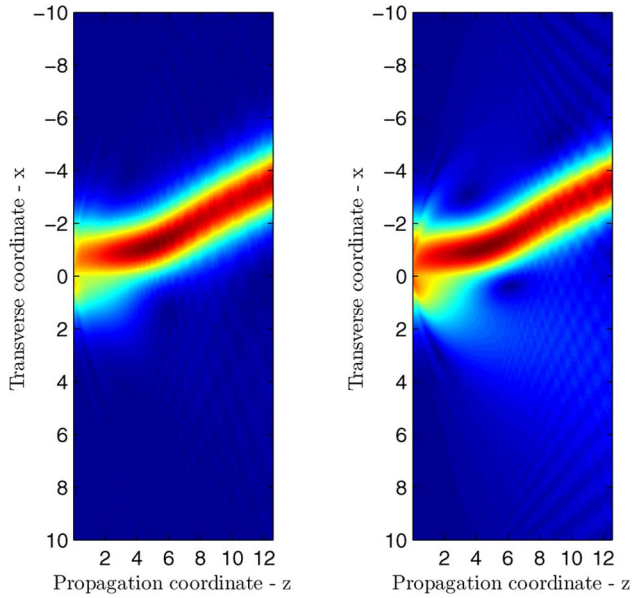

Fig. 7. (Color online) Same as in Fig. 5, but for the evolution of the unstable double-humped soliton, given by Eqs. (42)–(44) with initial scaled wavenumber $k = 1$ and $Q = -3$, pinned to the nonlinear layer of width 7.07 μm. The total propagation distance corresponding to this figure is $z = 100$ cm.

The substitution of the ansatz in Eq. (45) into Eqs. (40), (41), (11), and (12) produces the following results; cf. Eqs. (43) and (44):

$$k = -Q/3, \qquad W = \sqrt{-Q/6}, \qquad A' = \pm\sqrt{2}B', \qquad B' = +Q/(2\Gamma), \tag{46}$$

$$\sinh(2W\xi') = -\sqrt{-3Q/2}(\gamma/\Gamma). \tag{47}$$

The solution in Eq. (42) is nonsingular provided that Eq. (47) yields $\xi' > 0$, which is the case for the opposite signs of Γ and γ.

To better understand the meaning of these exact solutions, it is instructive to consider the NLS equation that corresponds to the cascading limit of Eqs. (40) and (41):

$$iu_z + (1/2)u_{xx} + [\tilde{\Gamma} + \tilde{\gamma}\delta(x)]|u|^2 u = 0, \tag{48}$$

$\tilde{\Gamma} \equiv \Gamma^2/(2Q)$, $\tilde{\gamma} \equiv \gamma\Gamma/Q + \gamma^2/(2Q) \int_{-\infty}^{+\infty} [\tilde{\delta}(x)]^2 dx$ [recall $\tilde{\delta}(x)$ is the regularized δ function of Eq. (6), cf. Eq. (20)]. In the case of $\tilde{\Gamma} > 0$, i.e., $Q > 0$, the exact solution to Eq. (48), which is the counterpart of the solution in Eq. (42), is

$$u = \sqrt{2k/\tilde{\Gamma}} e^{ikz} \mathrm{sech}\left(\sqrt{2k}(|x| + \xi)\right), \qquad \sinh\left(2\sqrt{2k}\xi\right) = 2(\tilde{\gamma}/\tilde{\Gamma})\sqrt{2k}, \tag{49}$$

where $k > 0$ is the respective wavenumber. The solution in Eq. (49) is valid for both positive and negative $\tilde{\gamma}$, i.e., respectively, the attractive and repulsive nonlinear defect in Eq. (48). The power of the solution in Eq. (49) is

$$P = \int_{-\infty}^{+\infty} |u(x)|^2 \mathrm{d}x = |\tilde{\gamma}|^{-1} \left[(2|\tilde{\gamma}|/\tilde{\Gamma})\sqrt{2k} - \mathrm{sgn}(\Gamma)\sqrt{8(\tilde{\gamma}/\tilde{\Gamma})^2 k + 1} + 1 \right]. \tag{50}$$

It immediately follows from this expression that, for either sign of $\tilde{\gamma}$, this soliton family satisfies the VK criterion, $dP/dk > 0$, which suggests that the solution in Eq. (42) (with identical signs of γ and Γ) is stable in the general case too, when the cascading limit does not apply. As mentioned above, this expectation was corroborated by direct simulations (not shown here).

The cascading-limit counterpart of the solution in Eq. (45) corresponds to $\tilde{\Gamma} < 0$, $\tilde{\gamma} > 0$. The respective exact solution to Eq. (48) and its power are

$$u = \sqrt{2k/|\tilde{\Gamma}|} e^{ikz} \left[\sinh\left(\sqrt{2k}(|x| + \xi)\right) \right]^{-1}, \qquad \sinh\left(2\sqrt{2k}\xi\right) = 2(\tilde{\gamma}/|\tilde{\Gamma}|)\sqrt{2k}, \tag{51}$$

$$P = \tilde{\gamma}^{-1} \left[\sqrt{8(\tilde{\gamma}/\tilde{\Gamma})^2 k + 1} - (2\tilde{\gamma}/\tilde{\Gamma})\sqrt{2k} + 1 \right]. \tag{52}$$

Equation (52) does not satisfy the VK criterion, as it yields $dP/dk < 0$, suggesting an instability of Eq. (45) in the absence of the cascading limit. Indeed, direct simulations of Eqs. (40) and (41) confirm that this solution is unstable, as shown in Fig. 8.

B. Linear Layer Embedded into the Self-Defocusing Nonlinear Medium (the Cascading Limit)

The existence of the solution in Eq. (51) to the asymptotic NLS Eq. (48) suggests considering a similar solution for a linear attractive layer (i.e., a usual waveguiding channel) embedded into the medium with the uniform self-defocusing cubic nonlinearity (in previous works, solitons pinned by the attractive defect were considered in the NLS equation with the self-focusing nonlinearity [22,23]). In terms of the $\chi^{(2)}$ system, this solution corresponds to the narrow linear channel in the limit of the large negative mismatch. The respective version of the NLS equation is

$$iu_z + (1/2)u_{xx} + \Gamma|u|^2u + \gamma_0\delta(x)u = 0, \tag{53}$$

with $\Gamma < 0$ and $\gamma_0 > 0$. In fact, we can fix $\Gamma \equiv -1$ in this case; then, an exact solution to Eq. (53) for a mode pinned by the attractive layer, is [cf. Eq, (51)]

$$u = \sqrt{2k}e^{ikz}\left[\sinh\left(\sqrt{2k}(|x| + \xi)\right)\right]^{-1},$$
$$\tanh\left(\sqrt{2k}\xi\right) = \sqrt{2k}/\gamma_0, \tag{54}$$

with power $P = \gamma_0 - \sqrt{2k}$, which features $dP/dk < 0$, formally contradicting the VK criterion. However, this criterion is not relevant for models with the self-defocusing nonlinearity. Actually, an argument in favor of the stability of Eq. (54) is the fact that its energy is negative:

$$E \equiv \frac{1}{2}\int_{-\infty}^{+\infty}[(u_x)^2 - u^4]\mathrm{d}x - \gamma_0u^2(x=0)$$
$$= -\left(\sqrt{2}/3\right)k^{3/2}\left(\gamma_0/\sqrt{2k} - 1\right)\left(2\gamma_0/\sqrt{2k} + 1\right)^2 \tag{55}$$

(recall $\Gamma = -1$ was fixed), hence the solution has a good chance to represent the ground state of the system. Direct simulations of Eq. (53) corroborate the stability of this pinned mode (not shown here).

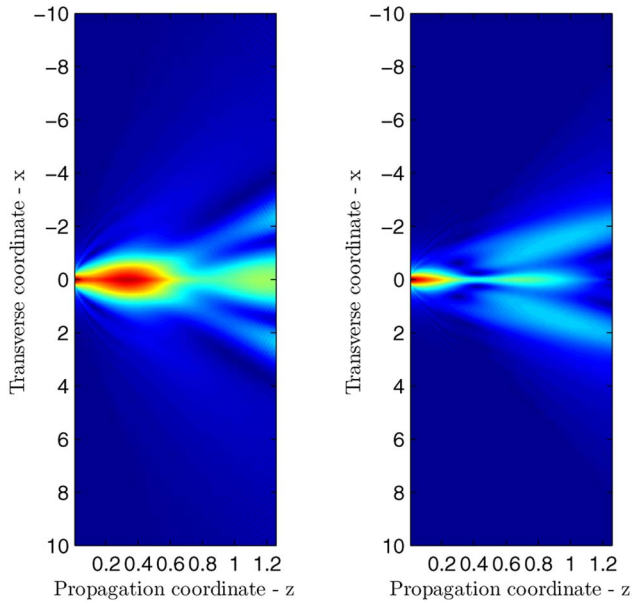

Fig. 8. (Color online) Same as in Fig. 7, but for the evolution of the unstable soliton, given by Eqs. (45)–(47) with initial scaled wavenumber $k = 1$ and $Q = -3$, pinned to the nonlinear layer of width 7.07 μm. The total propagation distance corresponding to this figure is $z = 10$ cm.

C. Two Embedded Layers

The extension of the model for the pair of symmetric layers is described by the following version of Eqs. (40) and (41) [cf. Eqs. (18) and (19) in the case of the linear host medium]:

$$iu_z + \frac{1}{2}u_{xx} + \left\{\Gamma + \gamma\left[\delta\left(x - \frac{L}{2}\right) + \delta\left(x + \frac{L}{2}\right)\right]\right\}u^*v = 0, \tag{56}$$

$$2iv_z + \frac{1}{2}v_{xx} - Qv + \frac{1}{2}\left\{\Gamma + \gamma\left[\delta\left(x - \frac{L}{2}\right) + \delta\left(x + \frac{L}{2}\right)\right]\right\}u^2 = 0. \tag{57}$$

A particular exact solution to Eqs. (56) and (57) can be found, in the form of a symmetric three-hump structure [with a maximum at $x = 0$, on the contrary to the double-humped solution in Eqs. (21) and (22), which has a minimum at $x = 0$], for the competing nonlinearities, $\Gamma > 0$, $\gamma < 0$:

$$u(x,z) = Ae^{-ikz}\begin{cases}\left[\cosh\left(\sqrt{-Q/6}(|x| - L)\right)\right]^{-2}, & \text{at } |x| > L/2,\\ \left[\cosh\left(\sqrt{-Q/6}x\right)\right]^{-2}, & \text{at } |x| < L/2,\end{cases} \tag{58}$$

$$v(x,z) = Be^{-2ikz}\begin{cases}\left[\cosh\left(\sqrt{-Q/6}(|x| - L)\right)\right]^{-2}, & \text{at } |x| > L/2,\\ \left[\cosh\left(\sqrt{-Q/6}x\right)\right]^{-2}, & \text{at } |x| < L/2,\end{cases} \tag{59}$$

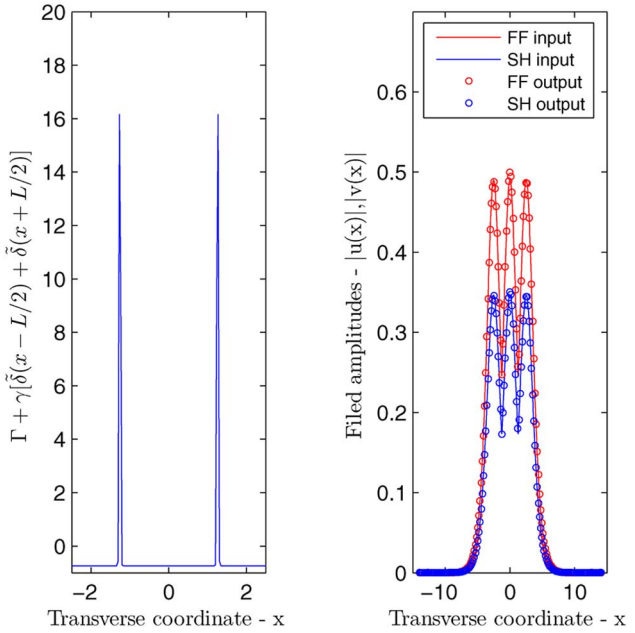

Fig. 9. (Color online) Left, the total nonlinearity coefficient, with the separation of $L = 200\,\mu$m, in physical units, between the two symmetric layers of width $a = 1.77\,\mu$m each. Right, a stable three-humped solution given by Eqs. (58) and (59), for $Q = -3$, $k = 1$, and $z = 100$ cm.

where k, A, and B are given by the same expressions in Eq. (43) as in the case of the solution in Eq. (42).

The highly degenerate nature of this solution is demonstrated by the fact that it satisfies the jump conditions in Eqs. (11) and (12) at points $x = \pm L/2$ at a single value of the strength of the localized nonlinearity, $\gamma = (2\Gamma/\sqrt{-6Q})\sinh(\sqrt{-Q/6}L)$ (recall that both Q and γ are negative, while Γ is positive, in the present case). As for the stability of the three-hump mode, it may be expected that, with a maximum of the local power set between two repulsive nonlinear layers, it is definitely unstable at small distance L between the layers (when they tend to merge into a single repulsive element, see the instability in Fig. 7), but it may become stable at larger L, when the repulsion from the two separated layers traps the power maximum between them. These expectations have been corroborated by direct simulations of Eqs. (56) and (57). In particular, an example of the stable mode, for large separation $L = 200\,\mu$m, is displayed in Fig. 9 (this solution is stable against large perturbations, which is not shown here in detail).

6. CONCLUSION

We have produced several exact solutions for spatial solitons supported by the $\chi^{(2)}$ layers embedded into a linear or nonlinear planar waveguide. The most fundamental solution describes the full set of families of the symmetric, asymmetric, and antisymmetric double-humped modes supported by the symmetric pair of the nonlinear layers inserted into the linear medium. The exact solutions describe the subcritical symmetry-breaking bifurcation in this system. In addition, particular exact solutions of several types were found for nonlinear stripes running through the nonlinear medium, including the case of the competition between the uniform and localized $\chi^{(2)}$ nonlinearities. The stability of the pinned solitons was tested by means of direct numerical simulations. In the case of the pair of nonlinear stripes embedded into the linear waveguide, the character of the (in)stability completely agrees with general principles of the bifurcation theory. For the layers embedded into the nonlinear host medium, the results for the stability were explained too, with the help of the consideration of the cascading limit.

The theoretical results reported in this paper call for an experimental realization. As an example, for a small phase mismatch $\Delta k = 20\,\mathrm{m}^{-1}$ and a typical nonlinear coefficient of 13 pm/V, the input intensities required to observe the soliton in the case of the single embedded layer are about $10^9\,\mathrm{W/cm}^2$. Such intensities are feasible, as demonstrated in [24], provided that the necessary nonlinear pattern can be fabricated.

ACKNOWLEDGMENTS

N. Voloch-Bloch is an Eshkol Scholar from the Israeli Ministry of Science, Culture and Sport.

REFERENCES

1. J. D. Joannopulos, S. G. Johnson, J. N. Winn, and R. D. Meade, *Manipulating Light with Strongly Modulated Photonic Crystals: Molding the Flow of Light* (Princeton Univ. Press, 2008).
2. A. N. Poddubny and E. L. Ivchenko, "Photonic quasicrystalline and aperiodic structures," Physica E **42**, 1871–1895 (2010).
3. F. Lederer, G. I. Stegeman, D. N. Christodoulides, G. Assanto, M. Segev, and Y. Silberberg, "Discrete solitons in optics," Phys. Rep. **463**, 1–126 (2008).
4. Y. V. Kartashov, B. A. Malomed, and L. Torner, "Solitons in nonlinear lattices," Rev. Mod. Phys. **83**, 247–306 (2011).
5. B. A. Malomed, Z. H. Wang, P. L. Chu, and G. D. Peng, "Multichannel switchable system for spatial solitons," J. Opt. Soc. Am. B **16**, 1197–1203 (1999).
6. B. A. Malomed, D. Mihalache, F. Wise, and L. Torner, "Spatiotemporal optical solitons," J. Opt. B **7**, R53–R72 (2005).
7. B. A. Malomed and M. Ya. Azbel, "Modulational instability of a wave scattered by a nonlinear center," Phys. Rev. B **47**, 10402–10406 (1993).
8. M. Vakhitov and A. Kolokolov, "Stationary solutions of the wave equation in a medium with nonlinearity saturation," Radiophys. Quantum Electron. **16**, 783–789 (1973).
9. N. Dror and B. A. Malomed, "Solitons supported by localized nonlinearities in periodic media," Phys. Rev. A **83**, 033828 (2011).
10. T. Mayteevarunyoo, B. A. Malomed, and G. Dong, "Spontaneous symmetry breaking in a nonlinear double-well structure," Phys. Rev. A **78**, 053601 (2008).
11. E. Bulgakov, K. Pichugin, and A. Sadreev, "Symmetry breaking for transmission in a photonic waveguide coupled with two off-channel nonlinear defects," Phys. Rev. B **83**, 045109 (2011).
12. A. A. Sukhorukov and Y. S. Kivshar, "Spatial optical solitons in nonlinear photonic crystals," Phys. Rev. E **65**, 036609 (2002).
13. Y. Kominis, "Analytical solitary wave solutions of the nonlinear Kronig-Penney model in photonic structures," Phys. Rev. E **73**, 066619 (2006).
14. P. G. Kevrekidis, *The Discrete Nonlinear Schrödinger Equation: Mathematical Analysis, Numerical Computations, and Physical Perspectives* (Springer, 2009).
15. C. Etrich, F. Lederer, B. A. Malomed, T. Peschel, and U. Peschel, "Optical solitons in media with a quadratic nonlinearity," Prog. Opt. **41**, 483–568 (2000).
16. A. V. Buryak, P. Di Trapani, D. V. Skryabin, and S. Trillo, "Optical solitons due to quadratic nonlinearities from basic physics to futuristic applications," Phys. Rep. **370**, 63–235 (2002).
17. A. A. Sukhorukov, Y. S. Kivshar, and O. Bang, "Two-color nonlinear localized photonic modes," Phys. Rev. E **60**, R41–R44 (1999).
18. I. Dolev, A. Ganany-Padowicz, O. Gayer, A. Arie, J. Mangin, and G. Gadret, "Linear and nonlinear optical properties of MgO:$LiTaO_3$," Appl. Phys. B **96**, 423–432 (2009).
19. S. Ashihara, J. Nishina, T. Shimura, and K. Kuroda, "Femtosecond measurement of nonlinear refraction in periodically poled lithium tantalate," in *Nonlinear Guided Waves and Their Applications*, A. Sawchuk, ed., Vol. 80 of OSA Trends Optics Photonics (Optical Society of America, 2002), paper NLMD41.
20. G. Iooss and D. D. Joseph, *Elementary Stability and Bifurcation Theory* (Springer, 1980).
21. Yu. N. Karamzin and A. P. Sukhorukov, "Nonlinear interaction of diffracted light beams in a medium with quadratic nonlinearity: mutual focusing of beams and limitation on the efficiency of optical frequency converters," JETP Lett. **20**, 339–342 (1974).
22. X. D. Cao and B. A. Malomed, "Soliton-defect collisions in the nonlinear Schrödinger equation," Phys. Lett. A **206**, 177–182 (1995).
23. R. H. Goodman, P. J. Holmes, and M. I. Weinstein, "Strong NLS soliton-defect interactions," Physica D **192**, 215–248 (2004).
24. S. M. Saltiel, D. N. Neshev, R. Fischer, W. Krolikowski, A. Arie, and Y. S. Kivshar, "Generation of second-harmonic conical waves via nonlinear Bragg diffraction," Phys. Rev. Lett. **100**, 103902 (2008).